

Size-dependent conductivity-type inversion in Cu₂O nanoparticles

B. Balamurugan, I. Aruna, and B. R. Mehta*

Thin Film Laboratory, Department of Physics, Indian Institute of Technology Delhi, New Delhi 110016, India

S. M. Shivaprasad

Surface Physics Group, National Physical Laboratory, New Delhi 110012, India

(Received 3 July 2003; revised manuscript received 20 January 2004; published 29 April 2004)

X-ray photoemission spectroscopy and optical absorption studies have been carried out on Cu₂O nanoparticles prepared using the activated reactive evaporation technique. A strong shift of the valence band edge (from 0.7 to 1.8 eV) has been observed on reduction of the nanoparticle size from 20 nm to 4 nm. The size-dependent modifications in the energy level diagram and metal-Cu₂O nanoparticle Schottky junction characteristics confirm the observation of the inversion of conductivity type from *p*-type bulk conductivity to *n*-type conductivity in Cu₂O nanoparticles at lower dimensions. This study can initiate a further methodology for tailoring the semiconductor properties of a material by controlling the nanoparticle size.

DOI: 10.1103/PhysRevB.69.165419

PACS number(s): 73.22.-f, 73.63.Bd, 73.30.+y

Quantum confinement of carriers and enhanced surface effects at nanodimensions are expected to result in large modifications in the structural, optical, and electronic properties of nanoparticles.¹⁻⁴ Experimental as well as theoretical investigations of size-dependent optical properties of nanoparticles are widely reported. In comparison, there are very few reports on the electronic properties of the nanoparticles.⁵⁻⁷ Size-dependent changes in the electronic properties of semiconductor nanoparticles are not only important from the basic physics point of view but will have an important impact on the potential application of nanoparticles in electronic devices. In theoretical investigations, the modification of the electronic properties of nanoparticles has been studied by simulating the changes in the band structure or by calculating the binding energy of the dopant impurities as a function of nanoparticle size.⁸⁻¹⁰ The band structure of small clusters and nanoparticles has been simulated in various material systems like CdS, ZnS, GaP, and Si.⁸⁻¹⁰ The changes in the binding energy of various dopant atoms in Al_{1-x}Ga_xAs, ZnS, and CdS nanoparticles have been attributed to the decrease in dielectric constant with the reduction of nanoparticle size.⁸ In limited experimental reports, the basic band structure of semiconductor nanoparticles has been studied in terms of the size-dependent shift in the valence or conduction band edges.^{11,12} X-ray absorption and photoemission spectra have been used to measure the band edges of silicon nanoparticles, which show a shift of 0.70 eV and 0.35 eV in the valence band and conduction band edges, respectively, on reduction of size to 2 nm.¹¹ Similarly, a shift of 0.63 eV in the valence band edge with reduction in the nanoparticle size from 7 nm to 2.4 nm has been observed from the x-ray photoemission spectroscopy (XPS) studies on CdS nanoparticles, and this has been related to the quantum confinement and dielectric solvation effects at smaller sizes.¹² Investigations related to the effect of nanoparticle character or size on measurable semiconductor parameters like conductivity, carrier concentration, or conductivity type are scarcely reported and are preliminary in nature.⁵⁻⁷ In this communication, size-dependent modifications in the electronic nature of copper oxide (Cu₂O) nanoparticles have

been determined using two widely different techniques of XPS and Schottky junction characterization. Based on these results, an energy band diagram of copper oxide nanoparticles having sizes of 4 nm, 9 nm, and 20 nm has been proposed and compared with that of a coarse grained Cu₂O.

Cu₂O nanoparticle layers have been synthesized using the activated reactive evaporation (ARE) technique. The deposition technique and detailed structural and optical characterization of these layers have been described elsewhere.^{13,14} In the present study, three copper oxide nanoparticle film samples, namely, samples A1, A2, and A3, were investigated. During deposition, pressure was maintained at 5×10^{-3} Torr and the flow rates of oxygen and argon were kept constant as 10 SCCM and 15 SCCM, respectively. (SCCM denotes cubic centimeters per minute at STP.) The particle size in these samples was controlled by changing the substrate temperature, 30 °C for sample A1, 200 °C for sample A2, and 300 °C for sample A3. For carrying out XPS and Schottky junction characterization, Cu₂O nanoparticle layers were deposited on glass and indium tin oxide (ITO) coated glass substrates, respectively. The thickness of the nanoparticle samples measured using a Talystep (Taylor-Hobson, U.K.) is 800 Å. The electronic properties of the nanoparticle films were determined by using a Keithley 224 programmable current source and a Keithley 2182 nanovoltmeter. A glancing angle x-ray diffractometer (GAXRD; Geigerflex-D/max-RB-RU200, Rigaku) and transmission electron microscope (TEM; JEOL TEM 200 CX) were used to determine the size of the Cu₂O nanoparticles. A double beam UV-visible-near-IR spectrophotometer (Hitachi 330) was employed to measure the optical reflectance and transmittance of the Cu₂O nanoparticle films. An x-ray photoelectron spectrometer (Perkin Elmer 1257 using Mg *K*α radiation of $E = 1253.6$ eV and a hemispherical section analyzer with 25 meV resolution) was used to study the valence band electronic structure of the Cu₂O nanoparticle films. The full width at half maximum (FWHM) of the Mg *K*α line used for XPS analysis is 0.6 eV and thus the energy resolution is expected to be of the order of 0.06 eV (10% of the FWHM). Keeping this in view, the energy resolution in the binding

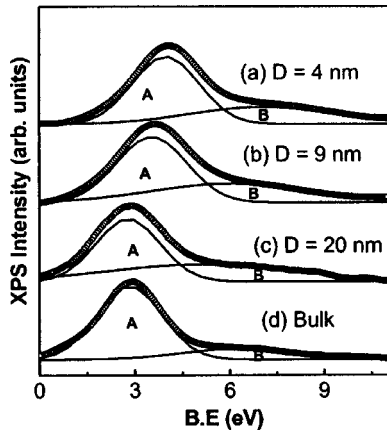


FIG. 1. Valence band x-ray photoemission spectra of the Cu_2O nanoparticle: curve *a*, sample A1 ($D=4$ nm), curve *b* sample A2 ($D=9$ nm), and curve *c*, sample A3 ($D=20$ nm). Curve *d* is for the bulk sample.

energy values obtained from the XPS analysis in the present study has been taken to be 0.1 eV. To compare the results of XPS and junction measurements on nanoparticle samples with bulk Cu_2O , a pellet of high-purity (99.99%) coarse grained Cu_2O powder having particle size greater than $5 \mu\text{m}$ (from Sigma Aldrich) was fabricated by pressing the powder in a hydrothermal process followed by annealing at 200°C . This sample will be referred to as the “bulk sample.” The average values of particle size estimated from the GAXRD studies are 4 nm, 9 nm, and 20 nm for samples A1, A2, and A3, respectively. The TEM micrographs show average particle sizes of 5 nm, 10 nm, and 22 nm for samples A1, A2, and A3, respectively. The values of nanoparticle size (D) estimated from the GAXRD measurement (4 nm, 9 nm, and 20 nm for samples A1, A2, and A3, respectively) will be used in the following discussion.

XPS valence band photoemission spectra of the Cu_2O nanoparticle film sample A1 ($D=4$ nm) after sputter removal of a 1.4 nm surface layer is shown in Fig. 1. The features in the XPS spectra shown in Fig. 1 correspond to the Cu_2O phase. In comparison to CuO (FWHM=3.9 eV), the valence band spectrum of Cu_2O is narrower (FWHM =2.3 eV) due to the splitting of the Cu 3*d* and O 2*p* peaks.¹⁵ The satellite feature on the higher-energy side at about 12–15 eV (which is a strong signature of the CuO phase) due to the deionization from the d^9 ground state to a d^8 -like final state is also absent in the XPS spectra (not shown in the figure). Glancing angle x-ray diffraction studies on these samples also show a single cubic Cu_2O phase. It may be mentioned that the Cu/O ratio stabilizes and remains constant (Cu/O=2) after the removal of about a 1.4 nm surface layer, and thus the XPS spectra in Fig. 1 correspond to the Cu_2O phase in the nanoparticle core. The FWHM of the Cu 3*d* peak and other signatures of the Cu_2O phase (absence of the satellite peak) remain unaltered during sputtering. This clearly shows that the Cu_2O phase in the nanoparticle core is stable and does not degrade on ion beam bombardment during depth profiling. As shown in Fig. 1, the XPS spectra of samples A1, A2, and A3 have been deconvoluted

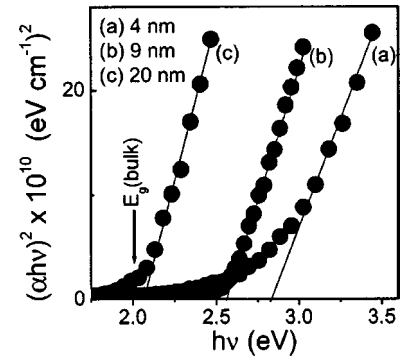


FIG. 2. Tauc plots showing the size-dependent blueshift in the band gap of Cu_2O nanoparticles.

into two peaks. Peaks A and B correspond to Cu 3*d* and O 2*p* XPS transitions, respectively. For comparison, the valence band XPS spectrum of the sputter-cleaned bulk sample is also given in Fig. 1. The Cu 3*d* XPS peak positions of the nanoparticle sample A3 ($D=20$ nm) and the bulk sample are observed at 2.9 eV, which is close to the reported value of 2.8 eV for bulk Cu_2O .¹⁵ The observed shift of 1.2 eV with respect to the bulk value on reduction of nanoparticle size to 4 nm is quite large as compared to the experimental resolution of 0.1 eV. The increase in binding energy of the Cu 3*d* XPS peak with decrease in particle size is due to the modified electronic structure at reduced dimensions. The increase in binding energy is a quantum confinement effect related to the broadening of the forbidden gap and can be explained in simple terms by the effective mass approximation.¹²

The optical absorption coefficient (α) of the Cu_2O nanoparticle films in the visible wavelength region ($0.35\text{--}0.85 \mu\text{m}$) has been determined from the transmittance, reflectance, and thickness data using a computer program based on Newton-Rapson’s iterative method following Tomlin’s algorithm.¹⁶ To estimate the optical absorption edge (E_g) in these films, the $(\alpha h\nu)^{1/n}$ vs $h\nu$ curves (Tauc plots) were plotted for different n values ($n=1/2, 3/2, 2, 3$). The best linear fit is obtained in the case of $n=1/2$, which indicates a direct allowed optical transition in copper oxide nanoparticles.¹⁷ The optical absorption edge has been determined from the intercept of the straight-line portion of the Tauc plots at $\alpha=0$. The Tauc plots given in Fig. 2 reveal an increase in the band gap from 2.04 eV to 2.9 eV with reduction in the nanoparticle size from 20 nm to 4 nm. As expected, the absorption edge of 2.04 eV for the 20 nm sample is equal to the reported value for bulk Cu_2O .¹⁸

The influence of size on the basic semiconducting nature of the Cu_2O nanoparticles has been further investigated by studying the size-dependent shift of the valence band edge in Cu_2O nanoparticles from the XPS results. The fitted Gaussian peaks corresponding to the Cu 3*d* transition in A1, A2, A3, and bulk samples are shown in Fig. 3. The Fermi level position is the zero point on the electron energy scale. The binding energy values are referenced to this point as the spectrometer work function and incident photon energy are known.¹⁹ The position of the valence band edge was obtained by extending the linear portion of the XPS peak to

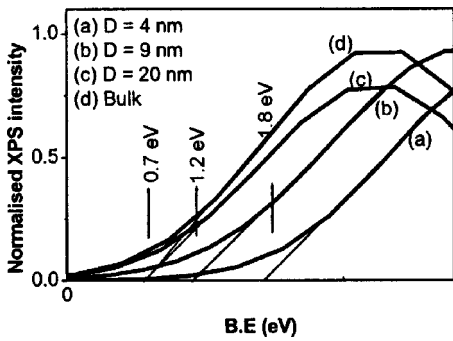


FIG. 3. Valence band x-ray photoemission spectra showing the size-dependent shift in the valence band edge in Cu₂O nanoparticles: curve *a*, sample A1 (*D* = 4 nm), curve *b*, sample A2 (*D* = 9 nm), and curve *c*, sample A3 (*D* = 20 nm). Curve *d* is the bulk sample.

zero intensity.^{11,12} These results clearly show a strong shift in the position of the valence band edge as a function of nanoparticle size. The valence band edge in the Cu₂O nanoparticle sample A2 (*D* = 9 nm) lies at 1.2 eV (curve *b*) and in the case of sample A1 (*D* = 4 nm) the valence band edge lies at 1.8 eV (curve *a*). On the other hand, the valence band edges in the Cu₂O nanoparticle sample A3 (*D* = 20 nm) and bulk sample lie at 0.7 eV (curves *c* and *d*, respectively). It may be mentioned that the valence band edge in the polycrystalline Cu₂O film has been reported at 0.64 eV below the Fermi level.²⁰

Energy level diagrams derived from the valence band and absorption edge values for the nanoparticle samples are shown in Fig. 4. For comparison, the energy level diagram of nanoparticle sample A3 and the bulk Cu₂O powder are also given in the figure. Using ΔE values (shift in the absorption edge value determined from the Tauc plot with respect to the bulk value), ΔE_V and ΔE_C values were calculated. Tight binding calculations in the case of Si nanoparticles have shown that the size-dependent valence band shift (ΔE_V) is larger than the conduction band shift (ΔE_C).^{10,11} In the absence of a better possibility, (ΔE_V)/(ΔE_C) values calculated for Si nanoparticles have been used for estimating ΔE_V and

ΔE_C for Cu₂O nanoparticles. In the case of Si nanoparticles the ratio is 2 at a particle size of 2 nm and increases to 3.5 with increase in the particle size to 3.6 nm. Further increase in the particle size results in a slight increase in the ratio to 4.^{10,11} Thus, we have taken the values of (ΔE_V)/(ΔE_C) equal to 3.5 and 4 for samples A1 (*D* = 4 nm) and A2 (*D* = 9 nm), respectively. The effect of nanoparticle size on the semiconductor character (conductivity type) can be described in terms of the position of the Fermi level in the energy level diagram. In the case of Cu₂O nanoparticle sample A3 (*D* = 20 nm) as well as the bulk sample with *p*-type conductivity, the Fermi level lies closer to the valence band at about 0.7 eV above the valence band edge. At a nanoparticle size equal to 9 nm, the Fermi level moves almost to the middle of the gap and on further reduction of nanoparticle size to 4 nm it becomes closer to the conduction band edge, indicating an inversion of conductivity from *p*-type bulk conductivity to *n*-type at lower nanoparticle sizes. The shift in the Fermi level position with reduction in particle size can be qualitatively explained as follows. Dopant binding energy calculations for nanoparticles has shown that a shallow dopant level becomes deep with reduction of particle size.⁸ It was also shown that in the case of semiconductor materials having a small Bohr excitonic radius (the Bohr excitonic radius for Cu₂O is 0.7 nm), the impurity level becomes exceptionally deep.^{8,21} The dopant ionization energy also depends on the dielectric constant of the semiconductor material as it shields the attractive force between the carrier (electron or hole) and the dopant ion.²² In the case of nanoparticles, the dielectric constant has been observed to decrease with a reduction of the particle size.⁸ A decrease in dielectric constant of the semiconductor material (ϵ) at reduced dimensions will thus result in an increase (by a factor of $1/\epsilon^2$) in the dopant ionization energy. The acceptor or donor energy levels become deep, resulting in the redistribution of the electron and hole concentrations in their corresponding bands which results in repositioning of the Fermi level. As already mentioned, the shift in the valence band edge at reduced dimensions is larger compared to the conduction band shift. Thus, the increase of dopant ionization

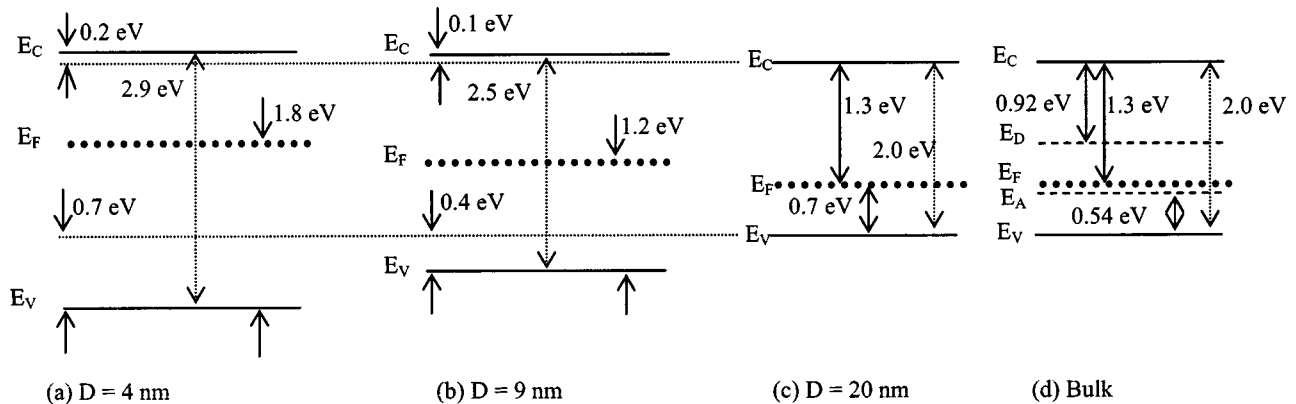


FIG. 4. Energy level diagram of Cu₂O nanoparticle: (a) sample A1, (b) sample A2, (c) sample A3, and (d) bulk sample. [The energy positions of acceptor levels due to copper vacancies and donor levels due to oxygen vacancies and band gap values for the bulk sample are taken from the literature (Ref. 20).]

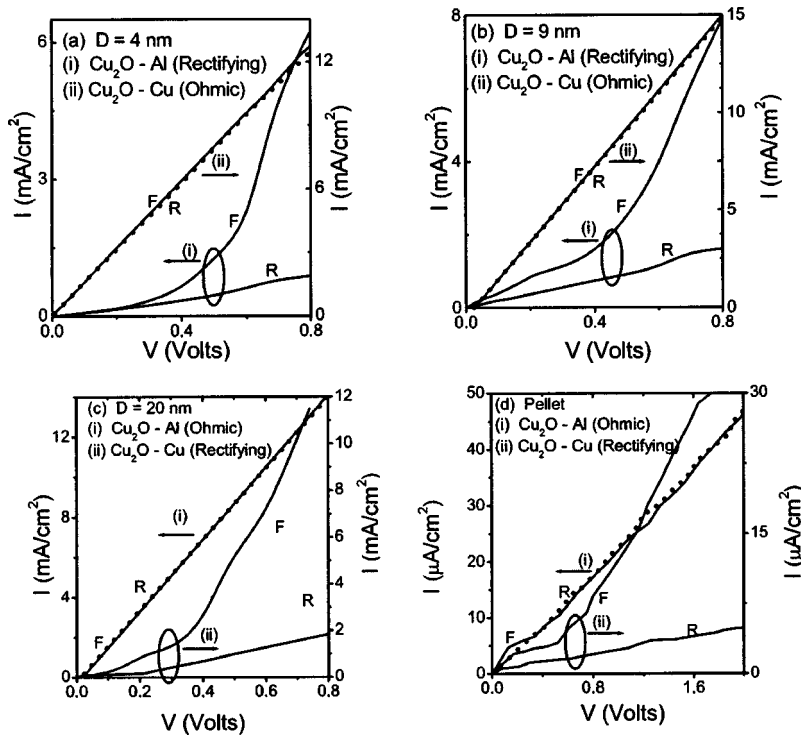


FIG. 5. I - V characteristics [forward (F) and reverse (R) bias] of Cu_2O -metal Schottky junctions for (a) nanoparticle sample A1, (b) nanoparticle sample A2, (c) nanoparticle sample A3, and (d) bulk.

energy (which is the difference in the energy of the dopant level and the corresponding band edge) is more pronounced for acceptor levels than donor levels. Thus the changes in the energy level diagram showing inversion of the conductivity type are due to the combined effect of (i) increase in the forbidden gap due to quantum confinement, (ii) difference in the valence and conduction band shifts, (iii) increase in the dopant ionization energy, and (iv) decrease in the dielectric constant, at lower nanoparticle sizes.

Schottky junction analyses of metal-copper oxide nanoparticle layers have been carried out to correlate the size-dependent modifications in the energy level diagram with the measurable electronic properties. The current-voltage (I - V) characteristics of Schottky junctions formed using Cu_2O nanoparticle films (samples A1 and A2) with aluminum (Al) and copper (Cu) contacts are shown in Figs. 5(a) and 5(b). In the case of nanoparticle samples A1 and A2, the I - V characteristics of Cu_2O -Al and Cu_2O -Cu junctions show good rectifying and Ohmic behavior, respectively. The linear I - V characteristic of the Cu_2O junction with Cu and the rectifying behavior of the Cu_2O junction with an Al metal contact indicate that the Cu_2O -ITO contact is Ohmic and the rectifying I - V behavior in the case of ITO- Cu_2O -Al is due to the Schottky junction formed at the Cu_2O -Al interface. On the other hand, nanoparticle Cu_2O sample A3 and the bulk sample [Figs. 5(c) and 5(d)] show rectifying behavior with Cu and Ohmic behavior with Al. This is opposite to what is observed in the case of nanoparticle samples A1 and A2 and points toward a change in the electronic character on reduction of nanoparticle size. It is important to note that on applying negative bias to the Cu_2O nanoparticle film with respect to the metal contact, a higher value of the current is observed, and this suggests an n -type semiconducting nature of the Cu_2O nanoparticle films in the case of samples A1 and

A2. In the case of sample A3 and the bulk sample, the semiconductor layer is positive with respect to Cu metal during forward bias. The difference in polarity during forward bias confirms that the difference in junction behavior is due to a change in conductivity type on reduction in nanoparticle size.

According to the Schottky-Mott theory for an ideal metal-semiconductor junction, a metal having a work function higher than a semiconductor results in a rectifying contact in the case of an n -type semiconductor and an Ohmic contact in the case of a p -type semiconductor. When the metal work function is lower than the semiconductor work function, the resulting contact is Ohmic and rectifying in the cases of n -type and p -type semiconductors, respectively.²³ It becomes difficult to apply the above mentioned simple theory as the reported work function values invariably depend on the surface conditions of the metal or semiconductor material.²⁴ More importantly, the behavior predicted by Schottky-Mott theory is strongly influenced by the presence of surface layers, nonstoichiometry at the semiconductor surface, chemical and physical interaction at the metal-semiconductor interface, or the presence of incomplete dangling bonds at the semiconductor surface. These factors make the barrier height of the metal semiconductor less sensitive and in many cases insensitive to the relative work function values of the metal and semiconductor materials.²³ In fact, it has been shown that in the case of polycrystalline Cu_2O the barrier height is in the range of 0.7–0.9 eV irrespective of the metal used.²⁵ Due to the increased surface area at nanodimensions, the influence of the surface on the junction characteristics can be more important in the case of nanoparticle films.

It is important to note that the junction behavior observed in the case of the bulk sample prepared from coarse grained powder and in sample A3 prepared by the ARE technique is

similar. Cu₂O polycrystalline films prepared using a variety of deposition techniques with varying growth temperature and growth ambient and thus having different surface conditions also show rectifying junctions with Cu and nonrectifying junctions with Al along with *p*-type conductivity.^{18,25–28} The junction behavior in terms of the rectifying/Ohmic nature and polarity during forward bias changes on reduction of the nanoparticle size from 20 nm to 9 nm. The nanoparticle film samples A1, A2, and A3 and the metal-semiconductor junction are prepared under similar conditions. This clearly shows that the observed conductivity type inversion is due to reduction of nanoparticle size and not due to any other effect. It has been reported that single-phase Cu₂O nanoparticles have a thin CuO-like surface modified layer.^{14,29} The presence of additional oxygen atoms at the surface may be a factor responsible for the passivation of surface and defect states, reducing the effect of surface states on the junction behavior. Passivation of defect states due to additional hydrogen in the case of silicon or metallic additives in the case of germanium is well known.^{30,31} The change in junction behavior on decreasing the particle size from 20 nm to 4 nm is thus related to the change in conductivity type on reduction of nanoparticle size. The changes in the energy level diagram derived from XPS and the optical absorption results support the conclusion of conductivity type inversion in-

ferred from the current-voltage behavior. The observation of inversion of conductivity type is important for device applications, as it is possible to form chemically compatible nanoparticle-polycrystalline homojunctions. This study also shows that the nanoparticle size may be a tool for tailoring the conductivity type and other semiconductor properties of materials.

In summary, based on the XPS and optical absorption results, energy level diagrams for Cu₂O nanoparticles having sizes of 4 and 9 nm have been proposed. These results show a strong shift of the Fermi level toward the conduction band edge, resulting in conductivity type inversion on reduction of nanoparticle size. This has been explained as due to a combined effect of the widening of the forbidden gap, the difference in the valence and conduction band shifts, the decrease in the dielectric constant, and the increase in the dopant binding energy at nanodimensions. This study shows a remarkable correlation between the measurable semiconductor characteristics and basic electronic changes in the energy level diagram of copper oxide nanoparticle films, and opens up a further methodology for controlling the semiconductor properties of materials by varying the nanoparticle size.

The authors B.B.M. and B.R.M. acknowledge the Ministry of Non-Conventional Energy Sources (MNES), Government of India for financial support of the present research.

*Author to whom correspondence should be addressed. Electronic address: brmehta@physics.iitd.ernet.in

¹S. Tsunekawa, K. Ishikawa, Z. Q. Li, Y. Kawazoe, and A. Kasuya, *Phys. Rev. Lett.* **85**, 3440 (2000).

²B. Balamurugan, B. R. Mehta, and S. M. Shivaprasad, *Appl. Phys. Lett.* **82**, 115 (2003).

³E. W. Draeger, J. C. Grossman, A. J. Williamson, and G. Galli, *Phys. Rev. Lett.* **90**, 167402 (2003).

⁴B. Balamurugan, B. R. Mehta, A. K. Avasthi, F. Singh, A. K. Arora, T. Rajalakshmi, G. Raghavan, A. K. Tyagi, and S. M. Shivaprasad, *J. Appl. Phys.* **92**, 3304 (2002).

⁵K. K. Nanda and S. N. Sahu, *Appl. Phys. Lett.* **79**, 2743 (2001).

⁶P. Patsalas and S. Logotheddis, *J. Appl. Phys.* **90**, 4725 (2001).

⁷R. S. Ningthoujam, N. Sudhakar, K. P. Rajeev, and N. S. Gajbhiye, *J. Appl. Phys.* **91**, 6051 (2002).

⁸V. Ranjan and V. A. Singh, *J. Appl. Phys.* **89**, 6415 (2001).

⁹P. E. Lippens and M. Lannoo, *Phys. Rev. B* **39**, 10 935 (1989).

¹⁰S. Y. Ren and J. D. Dow, *Phys. Rev. B* **45**, 6492 (1992).

¹¹T. v. Buren, L. N. Dinh, L. L. Chase, W. J. Siekhaus, and L. J. Terminello, *Phys. Rev. Lett.* **80**, 3803 (1998).

¹²V. L. Colvin, A. P. Alivisatos, and J. G. Tobin, *Phys. Rev. Lett.* **66**, 2786 (1991).

¹³B. Balamurugan and B. R. Mehta, *Thin Solid Films* **396**, 90 (2001).

¹⁴B. Balamurugan, B. R. Mehta, and S. M. Shivaprasad, *Appl. Phys. Lett.* **79**, 3176 (2001).

¹⁵J. Ghijsen, L. H. Tjeng, J. van Elp, H. Eskes, J. Westerink, G. A. Sawatzky, and M. T. Czyzyk, *Phys. Rev. B* **38**, 11 322 (1988).

¹⁶S. G. Tomlin, *J. Phys. D* **1**, 1667 (1968).

¹⁷F. Wooten, *Optical Properties of Solids* (Academic Press, New York, 1972).

¹⁸A. E. Rakshani, *Solid-State Electron.* **29**, 7 (1986).

¹⁹C. D. Wagner, W. M. Riggs, L. E. Davis, J. F. Moulder, and G. E. Mullenberg, *Hand Book of X-Ray Photoelectron Spectroscopy* (Perkin-Elmer Corporation, Eden Prairie, MN, 1979).

²⁰A. E. Rakshani, *J. Appl. Phys.* **69**, 2365 (1991).

²¹S. Jana and P. K. Biswas, *Mater. Lett.* **32**, 263 (1997).

²²S. M. Sze, *Physics of Semiconductor Devices* (Wiley, Singapore, 2002).

²³B. L. Sharma, *Metal-Semiconductor Schottky Barrier Junctions and Their Applications* (Plenum Press, New York, 1984).

²⁴*CRC Handbook of Chemistry and Physics*, 82nd ed., edited by D. R. Lide (CRC Press, London, 2001).

²⁵B. P. Rai, *Solar Cells*, **25**, 265 (1988).

²⁶R. J. Iwanowski and D. Trivich, *Phys. Status Solidi A* **95**, 735 (1986).

²⁷T. Suehiro, T. Sasaki, and Y. Piratate, *Thin Solid Films* **383**, 318 (2001).

²⁸J. A. Assimos and D. Trivich, *J. Appl. Phys.* **44**, 1687 (1973).

²⁹K. Borgohain, N. Murase, and S. Mahamuni, *J. Appl. Phys.* **92**, 1292 (2002).

³⁰E. C. Freeman and W. Paul, *Phys. Rev. B* **18**, 4288 (1978).

³¹K. L. Chopra and P. Nath, *Phys. Status Solidi A* **33**, 333 (1976).